Available online at www.sciencedirect.com
SCIENCE DIRECT
Journal of Catalysis 233 (2005) 26–35
JOURNAL OF CATALYSIS
www.elsevier.com/locate/jcat

Kinetic modeling of nitrous oxide decomposition on Fe-ZSM-5 based on parameters obtained from first-principles calculations

Andreas Heyden [a,*], Alexis T. Bell [b,*], Frerich J. Keil [a]

[a] *Department of Chemical Engineering, Hamburg University of Technology, D-21073 Hamburg, Germany*
[b] *Department of Chemical Engineering, University of California, Berkeley, CA 94720-1462, USA*

Received 21 February 2005; revised 24 March 2005; accepted 6 April 2005

Available online 23 May 2005

Abstract

A reaction mechanism for the decomposition of N_2O on Fe-ZSM-5 has been proposed by Heyden et al. based on a detailed density functional theory analysis of the energetics for alternative pathways. This work suggested that isolated Fe cations bound to a single oxygen atom (viz., $Z^-[FeO]^+$) are the active sites for N_2O decomposition. It was also shown that the presence of water vapor in the feed stream to the catalyst can deactivate these sites, but this process was demonstrated to be reversible at temperatures above about 690 K. In the present work, the decomposition of N_2O was simulated under non-steady-state conditions using the mechanism of Heyden et al. and the rate coefficients calculated by these authors. These simulations closely reproduce the results of temperature-programmed reaction and pulsed N_2O decomposition experiments. The dynamics of water desorption from deactivated Fe sites are found to be slow. Thus at 773 K, dehydration of a fully hydrated sample of Fe-ZSM-5 can take up to 10 h. The present study also shows that temperature-programmed desorption of O_2 from Fe-ZSM-5 after N_2O decomposition arises from the reaction $Z^-[FeO_2]^+ \rightleftarrows Z^-[Fe]^+ + O_2$, but that this process is not a part of the mechanism for N_2O decomposition under steady-state conditions.

Keywords: N_2O decomposition; Fe-ZSM-5; Simulation; Kinetic modeling

1. Introduction

Fe-ZSM-5 is an active catalyst for the stoichiometric decomposition of N_2O to N_2 and O_2 [1–11] and is therefore potentially useful for the abatement of N_2O emissions from industrial waste streams, such as those occurring in nitric acid and adipic acid plants [12,13]. These findings have stimulated an interest in identifying the nature of the active site for N_2O decomposition and the mechanism via which this reaction occurs.

The state of iron in Fe-ZSM-5 is strongly dependent on the method of iron exchange, the level of Fe exchange (i.e., the Fe/Al ratio), and the pretreatment of the as-exchanged material [14–25]. In general, it is agreed that tetragonally coordinated iron ions in the zeolite framework and iron oxide particles at the external surface of the zeolite crystal are inactive for N_2O decomposition. Careful preparation of Fe-ZSM-5 by dry exchange of H-ZSM-5 minimizes the formation of Fe_3O_4 nanoparticles and enhances the dispersion of Fe. EXAFS characterization of such materials has provided evidence for both diferric oxo/hydroxyl-bridged clusters [15–21] and isolated ferric oxo species [14,22,23]. Fe cations can also be incorporated into the zeolite framework during synthesis. If the resulting framework also contains tetrahedrally coordinated Al atoms, then upon high-temperature pretreatment Fe atoms leave the zeolite framework and are stabilized as extra-framework FeO species at cation exchange positions associated with the framework Al [23]. EXAFS characterization of Fe-ZSM-5 prepared by dry exchange of H-ZSM-5 and high-temperature treatment of Fe/Al-MFI shows that the environment of Fe is effectively the same and is best described as isolated Fe cations [23].

* Corresponding authors.
E-mail addresses: a.heyden@tuhh.de (A. Heyden), bell@cchem.berkeley.edu (A.T. Bell).

0021-9517/$ – see front matter
doi:10.1016/j.jcat.2005.04.003

Van Santen and co-workers [26,27] have pointed out that a minority species could be responsible for catalysis. Pérez-Ramírez et al. [28] and Pirnburger et al. [29] have concluded from studies of N_2O decomposition kinetics that mononuclear iron species exhibit the highest activity per mole of iron, and highly clustered species exhibit the lowest activity. Since differently prepared zeolites lead to different types of iron species but show qualitatively similar catalytic behavior in N_2O decomposition, Pirngruber et al. [29] have suggested that the same iron species is present in all samples, but in different concentrations.

Heyden et al. [30] have recently reported the results of a density functional theory (DFT) investigation of the mechanism of the nitrous oxide decomposition on hydrated and dehydrated mononuclear iron sites in Fe-ZSM-5. Isolated Fe cations in the form of $Z^-[FeO]^+$ were found to be the most active centers for N_2O decomposition. An important part of the investigation was the determination that very low concentrations of water strongly affect the speciation of Fe in Fe-ZSM-5. It was demonstrated that $Z^-[FeO]^+$ sites react with water to form $Z^-[Fe(OH)_2]^+$, which is inactive for N_2O decomposition but can be decomposed back to $Z^-[FeO]^+$ at elevated temperatures above 690 K. Water concentrations in the range of ppb to ppm were found to have a significant effect on the distribution of iron species and on the apparent activation energy and preexponential factor in the temperature range from 600 to 700 K, where most kinetic studies are performed. At 600 K nearly all active mononuclear iron sites are poisoned with water, and at 700 K water desorbs and the majority of the single iron sites are active. It was shown that the spread in the values of the rate parameters reported by different research groups is likely a reflection of the influence of water vapor in the feed stream.

The purpose of the present study is to show that the mechanism and rate parameters reported in our earlier work [30] can be used to provide insights into the effects of water vapor on experimental observations, particularly those obtained from temperature-programmed reaction (TPR), transient response, and temperature-programmed desorption (TPD) experiments conducted with Fe-ZSM-5. The model of N_2O decomposition kinetics is also used to address the issue of whether O_2 desorption is rate-limiting, as has been suggested by several authors [11,31–33].

2. Mechanism and kinetics of N_2O decomposition over Fe-ZSM-5

A comprehensive analysis of alternative pathways for the decomposition of N_2O on isolated Fe sites in Fe-ZSM-5 leads to the conclusion that the preferred reaction mechanism is that shown in Fig. 1 [30]. As shown in the supplementary materials to this paper, the rate of N_2O decomposition can be written as

$$r_{N_2O} = k_{app} P_{N_2O}. \tag{1}$$

The apparent rate coefficient appearing in Eq. (1) can be expressed as

$$k_{app} = \frac{2(k_4 + k_{11})K_3}{\left(1 + K_1K_2P_{H_2O} + \frac{(k_4+k_{11})K_3}{k_6K_5+k_{13}K_{12}K_{14}}\right)}. \tag{2}$$

Similarly, it is possible to express the fraction of the isolated Fe sites that are present as $Z^-[FeO]^+$, $Z^-[FeO_2]^+$, and $Z^-[Fe(OH)_2]^+$ in the following manner:

$$\Theta_{FeO} = \frac{1}{\left(1 + K_1K_2P_{H_2O} + \frac{(k_4+k_{11})K_3}{k_6K_5+k_{13}K_{12}K_{14}}\right)}, \tag{3}$$

$$\Theta_{FeO_2} = \frac{(k_4 + k_{11})K_3}{k_6K_5 + k_{13}K_{12}K_{14}}\Theta_{FeO}, \tag{4}$$

$$\Theta_{Fe(OH)_2} = K_1K_2\Theta_{FeO}P_{H_2O}. \tag{5}$$

The rate coefficients and equilibrium constants appearing in Eqs. (1)–(5) are listed in Table 1.

3. Results and discussion

3.1. Effects of water vapor on the distribution of Fe species and the rate of N_2O decomposition

As noted previously [30], small amounts of water vapor can strongly affect the apparent first-order rate coefficient for N_2O decomposition and the fractional distribution of Fe among the species $Z^-[FeO]^+$, $Z^-[FeO_2]^+$, and $Z^-[Fe(OH)_2]^+$. For example, at 700 K the apparent rate constant decreases by a factor of 2.7 if the steady-state water pressure is 10^{-6} bar (compared with a water-free catalytic system), whereas at 600 K the apparent rate constant decreases by a factor of 360. Fig. 2 shows the effects of water on the distribution of $Z^-[FeO]^+$, $Z^-[FeO_2]^+$, and $Z^-[Fe(OH)_2]^+$ at 700 and 600 K. At 700 K, traces of water in the range of 10^{-9} to 10^{-6} bar have very little effect on the fraction of catalytically active sites ($Z^-[FeO]^+$ and $Z^-[FeO_2]^+$), whereas at 600 K the fraction of active sites decreases significantly if the water pressure is higher than 10^{-8} bar.

Experimental measurements of the apparent activation energy and preexponential factor for N_2O decomposition are most often made over the temperature range of 500–700 K, and in this temperature interval low concentrations of water vapor in the feed stream can have a very strong effect on the apparent rate parameters. As shown in Fig. 3, the reported values of the apparent preexponential factor correlate with the apparent activation energy over a wide range of values. Virtually all of this variation can be attributed to the effects of small amounts of water vapor in the feed. The solid line in Fig. 3 shows the correlation between the apparent preexponential factor and the apparent activation energy predicted on the basis of the mechanism presented in Fig. 1 and the values of the rate and equilibrium parameters listed in Table 1. A temperature interval of 600–700 K was used for

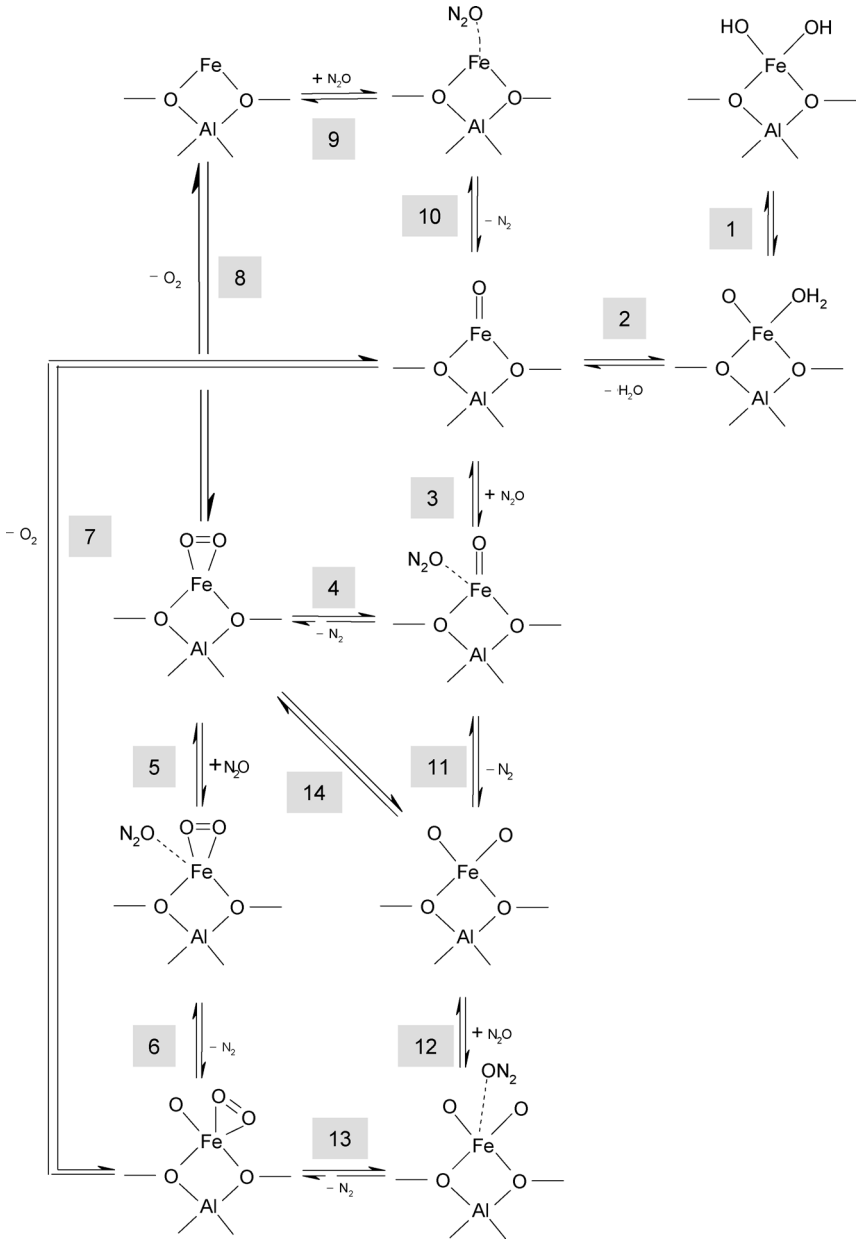

Fig. 1. Reaction network of the N_2O dissociation on mononuclear iron oxo species and poisoning of single iron sites with water molecules.

these calculations. The lowest preexponential factor and activation energy are calculated for a zero partial pressure of water, and the highest values are calculated for an assumed water vapor partial pressure of 10^{-7} bar. It is evident that the differences in the concentration of water vapor in the feed can readily account for the wide variation in the apparent rate parameters determined from experimental data. The absence of full agreement between the theoretical line and some of the data may be due to the following two reasons. One is that not all of the iron in the zeolite may be in the form of isolated Fe sites. If the fraction of iron present as isolated sites is less than unity, this would lead to a systematic underestimation of the preexponential factor. The other factor contributing to the absence of full agreement is the temperature interval over which the apparent activation energy was determined. As discussed below, if the temperature interval is large and centered around lower temperatures, the calculated apparent activation energy will be large. These factors might explain why the data of Pirngruber et al. [34] and Roy et al. [35] lie below the theoretical line and the rest of the experimental data.

3.2. Simulation of temperature-programmed reaction experiments

A simulation of the temperature-programmed reaction experiment reported by Wood et al. [31] was performed to further validate the mechanism presented in Fig. 1 and the kinetics of N_2O decomposition represented by Eq. (1). This work was chosen because the investigators had carried

Table 1
Computed reaction enthalpy, activation barriers, preexponential factors for equilibrium constants and preexponential factors for forward reaction for each elementary step in nitrous oxide dissociation in Fe-ZSM-5

Reaction	Reaction No. used by Heyden et al. [30]	$E^{\ddagger}$, ΔH[a] (kcal/mol)	Constant	T (K)		
				600	700	800
1. $Z^-[FeO]^+(OH_2)\ \{M=6\}$	63	$\Delta H_1 = -27.1$	K_1^0, –	2.43E−01	2.43E−01	2.44E−01
$\rightleftarrows Z^-[Fe(OH)_2]^+\ \{M=6\}$		$E_1^{\ddagger} = 9.2$	A_1, s^{-1}	2.28E+12	2.18E+12	2.13E+12
2. $Z^-[FeO]^+\ \{M=6\} + H_2O(g)$	61	$\Delta H_2 = -15.6$	K_2^0, bar^{-1}	5.32E−07	4.76E−07	4.53E−07
$\rightleftarrows Z^-[FeO]^+(OH_2)\ \{M=6\}$		$E_2^{\ddagger} = 0.0$	A_2, $s^{-1}\,bar^{-1}$	1.58E+06	2.03E+06	2.57E+06
3. $Z^-[FeO]^+\ \{M=6\} + N_2O(g)$	23	$\Delta H_3 = -4.8$	K_3^0, bar^{-1}	1.70E−06	1.67E−06	1.69E−06
$\rightleftarrows Z^-[FeO]^+(ON_2)\ \{M=6\}$		$E_3^{\ddagger} = 0.0$	A_3, $s^{-1}\,bar^{-1}$	5.75E+06	7.95E+06	1.06E+07
4. $Z^-[FeO]^+(ON_2)\ \{M=6\}$	36	$\Delta H_4 = -20.0$	K_4^0, bar	9.12E+05	9.30E+05	9.26E+05
$\rightleftarrows Z^-[FeO_2]^+\ \{M=6\} + N_2(g)$		$E_4^{\ddagger} = 30.4$	A_4, s^{-1}	5.40E+13	6.22E+13	6.98E+13
5. $Z^-[FeO_2]^+\ \{M=6\} + N_2O(g)$	24	$\Delta H_5 = -1.2$	K_5^0, bar^{-1}	6.31E−07	6.19E−07	6.27E−07
$\rightleftarrows Z^-[FeO_2]^+(ON_2)\ \{M=6\}$		$E_5^{\ddagger} = 0.0$	A_5, $s^{-1}\,bar^{-1}$	2.19E+06	3.01E+06	3.99E+06
6. $Z^-[FeO_2]^+(ON_2)\ \{M=6\}$	38	$\Delta H_6 = -12.0$	K_6^0, bar	1.62E+01	3.74E+01	6.52E+01
$\rightleftarrows Z^-[O_2FeO]^+\ \{M=6\} + N_2(g)$		$E_6^{\ddagger} = 20.1$	A_6, s^{-1}	5.91E+09	1.56E+10	3.12E+10
7. $Z^-[O_2FeO]^+\ \{M=6\}$	53	$\Delta H_7 = -0.6$	K_7^0, bar	8.21E+07	8.33E+07	8.21E+07
$\rightleftarrows Z^-[FeO]^+\ \{M=6\} + O_2(g)$		$E_7^{\ddagger} = 8.0$	A_7, s^{-1}	1.25E+13	1.46E+13	1.67E+13
8. $Z^-[FeO_2]^+\ \{M=6\}$	51	$\Delta H_8 = 52.1$	K_8^0, bar	6.50E+06	6.66E+06	6.59E+06
$\rightleftarrows Z^-[Fe]^+\ \{M=6\} + O_2(g)$		$E_8^{\ddagger} = 54.2$	A_8, s^{-1}	1.25E+13	1.46E+13	1.67E+13
9. $Z^-[Fe]^+\ \{M=6\} + N_2O(g)$	22	$\Delta H_9 = 1.9$	K_9^0, bar^{-1}	1.04E−03	1.02E−03	1.03E−03
$\rightleftarrows Z^-[Fe]^+(ON_2)\ \{M=6\}$		$E_9^{\ddagger} = 0.03$	A_9, $s^{-1}\,bar^{-1}$	2.69E+09	3.86E+09	5.30E+09
10. $Z^-[Fe]^+(ON_2)\ \{M=6\}$	29	$\Delta H_{10} = -67.9$	K_{10}^0, bar	5.02E+03	5.11E+03	5.09E+03
$\rightleftarrows Z^-[FeO]^+\ \{M=6\} + N_2(g)$		$E_{10}^{\ddagger} = 2.8$	A_{10}, s^{-1}	6.28E+09	6.36E+09	6.43E+09
11. $Z^-[FeO]^+(ON_2)\ \{M=6\}$	37	$\Delta H_{11} = -11.8$	K_{11}^0, bar	3.35E+05	3.38E+05	3.34E+05
$\rightleftarrows Z^-[OFeO]^+\ \{M=6\} + N_2(g)$		$E_{11}^{\ddagger} = 30.7$	A_{11}, s^{-1}	1.58E+14	1.84E+14	2.09E+14
12. $Z^-[OFeO]^+\ \{M=6\} + N_2O(g)$	25	$\Delta H_{12} = -3.0$	K_{12}^0, bar^{-1}	4.31E−07	4.22E−07	4.27E−07
$\rightleftarrows Z^-[OFeO]^+(ON_2)\ \{M=6\}$		$E_{12}^{\ddagger} = 0.0$	A_{12}, $s^{-1}\,bar^{-1}$	1.51E+06	2.07E+06	2.74E+06
13. $Z^-[OFeO]^+(ON_2)\ \{M=6\}$	39	$\Delta H_{13} = -18.3$	K_{13}^0, bar	3.08E+06	3.13E+06	3.11E+06
$\rightleftarrows Z^-[O_2FeO]^+\ \{M=6\} + N_2(g)$		$E_{13}^{\ddagger} = 16.5$	A_{13}, s^{-1}	2.35E+14	2.81E+14	3.25E+14
14. $Z^-[FeO_2]^+\ \{M=6\}$	59	$\Delta H_{14} = 8.1$	K_{14}^0, –	3.37E−01	3.38E−01	3.39E−01
$\rightleftarrows Z^-[OFeO]^+\ \{M=6\}$		$E_{14}^{\ddagger} = 22.5$	A_{14}, s^{-1}	7.68E+12	8.11E+12	8.46E+12

$E^{\ddagger}$, calculated activation energy including zero-point energy correction.
[a] Calculated enthalpy averaged over 600–800 K.

out their studies with a carefully prepared sample of Fe-ZSM-5 (Si/Al = 84 and Fe/Al = 0.38), which was shown by EXAFS to contain primarily isolated Fe cations [23]. Before initiating a TPR experiment, Wood et al. [31] pretreated 100 mg of catalyst (6.79×10^{-6} mol Fe) at 773 K in 3.0% N_2O and then cooled the catalyst to 298 K. The catalyst was then exposed to a flow of 15,000 ppm N_2O in He (total flow rate, 60 cm^3/min; reactor volume, 0.112 cm^3) while the temperature was increased at 5 K/min from 298 to 773 K. The amount of iron and the N_2O feed flow rate used in the simulation were the same as those used in the experimental work. Since it is not known what fraction of the Fe in the sample used by Wood et al. [31] was present as isolated sites and what was the feed concentration of water vapor, these parameters were varied to get the best fit between the experimentally observed and simulated N_2 partial pressures. To achieve this fit, the function $F(P_{H_2O}, f) = \Sigma(P_{N_2}^{exp} - P_{N_2}^{sim})^2$ was minimized.

For the simulations, it was assumed that the iron in the catalyst occurs in two forms, inactive iron clusters and single iron sites, that are active for N_2O decomposition or are poisoned by water molecules. The fraction of iron present as isolated sites is defined as f. The reactor used by Wood et al. [31] was modeled as a CSTR, since the catalyst bed is shallow and, hence, considerable back-mixing is expected. It was also assumed that the surface composition reaches steady state at each temperature and that the rate of reaction is not diffusionally limited. The latter assumption was supported by estimates of the Thiele modulus, which remains less than 0.2 for temperatures up to 773 K. Under these conditions, the partial pressures of O_2, N_2, and N_2O can be calculated at every temperature T as

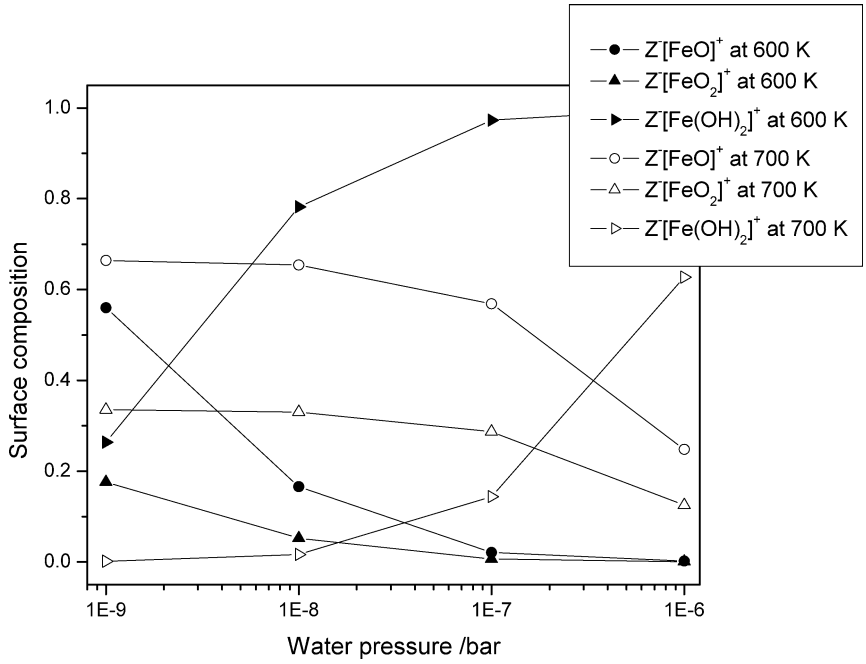

Fig. 2. Surface composition of single iron species under reaction condition at a temperature of 600 and 700 K. $Z^-[FeO]^+$ is the active site for N_2O decomposition on Fe-ZSM-5. $Z^-[FeO_2]^+$ is the one time oxidized active site (possible α-O site), $Z^-[Fe(OH)_2]^+$ is the inactive single iron site in Fe-ZSM-5.

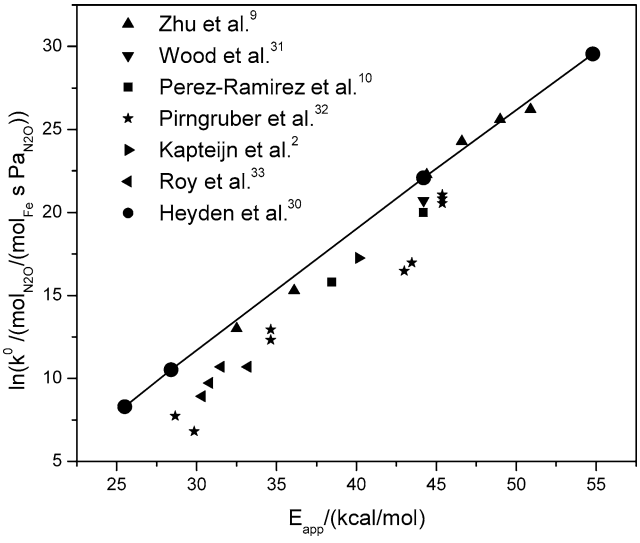

Fig. 3. Plot of logarithm of experimental and computed apparent preexponential factor versus apparent activation barrier.

$$P_{N_2O} = P^0_{N_2O} \exp\left(-\frac{f N_{Fe} RT}{V} k_{app}\tau\right), \quad (6)$$

$$P_{N_2} = 2P_{O_2} = P^0_{N_2O} - P_{N_2O}, \quad (7)$$

where V is the reactor volume, τ is the residence time, R is the ideal gas constant, $f N_{Fe}$ is the total amount of single iron atoms in the catalyst, and k_{app} is the apparent rate coefficient given by Eq. (1). An optimization algorithm for unconstrained minimizations of a sum of squares was used to determine the fraction of single iron sites and the partial pressure of water in the feed [36]. Fig. 4a illustrates the close agreement between the experimental and simulated TPR profiles. The best fit was obtained with $f = 0.544$ and a partial pressure of water in the feed stream of 406×10^{-9} bar.

Eq. (1) leads to the conclusion that an Arrhenius plot of the apparent first-order rate coefficient for N_2O decomposition will not be linear and will depend on the partial pressure of water vapor in the feed. This expectation is confirmed by Fig. 4b. The experimental data of Wood et al. [31] also fail to plot as a straight line. Although the agreement between simulation and experiment is excellent at high temperatures, at temperatures below 670 K the experimental value of the apparent rate coefficient exceeds that determined from the simulation. A possible cause for this discrepancy might be that the catalyst surface is not in steady state. Because of the catalyst pretreatment more active iron sites appear to be available in the experiments than would be present in the simulation, which assumes that the distribution of adsorbed species reaches a steady state instantaneously. However, whatever the cause of the discrepancy, it is evident that the value of the calculated apparent activation energy is highly dependent on the temperature range used for the calculation and the water vapor concentration present in the feed (see Fig. 4).

A corollary to the preceding conclusion is that the water vapor content in the feed required to achieve a match between the experimentally observed and calculated apparent activation energies will be strongly dependent on the temperature range over which the activation energy is determined in the experimental study. For example, Heyden et al. [30] reported that the apparent activation barrier determined by Wood et al. [31] over the temperature range of 600 to 700 K, 44.2 kcal/mol, could be reproduced if the partial pressure of water in the feed were assumed to be 23×10^{-9} bar. However, this result appears to contra-

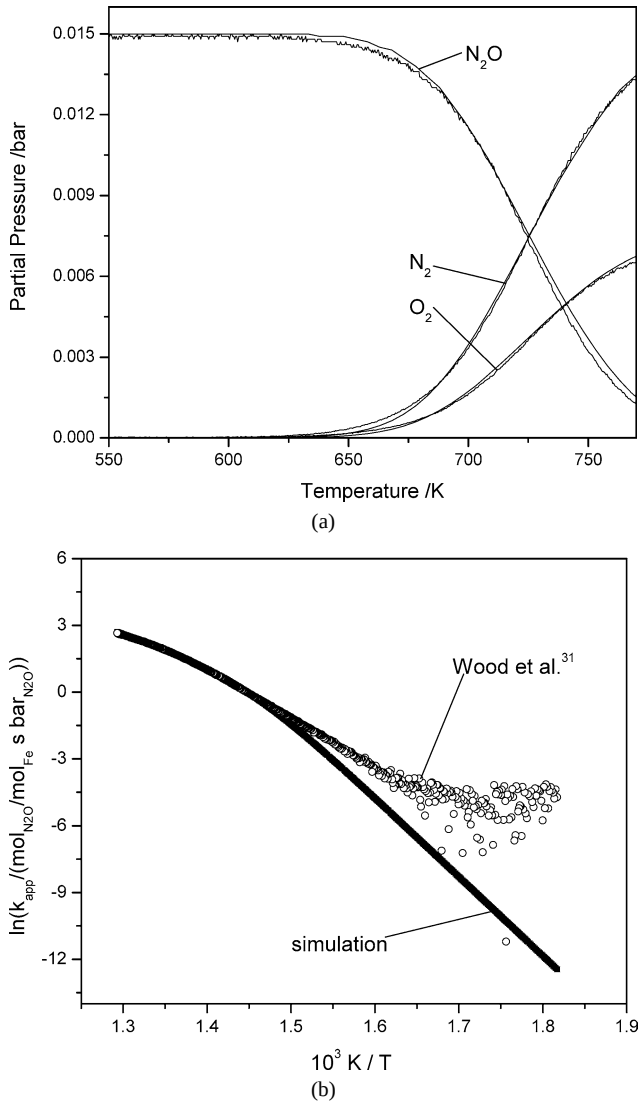

Fig. 4. (a) Experimental and simulated temperature programmed decomposition profile observed during the passage of 15,000 ppm N_2O in He over Fe-ZSM-5. The simulated TPR profile was obtained with an optimized single iron fraction of 0.544 (95% confidence interval: 0.541–0.546) and a water pressure of 406×10^{-9} bar (95% confidence interval: 396–416 $\times 10^{-9}$ bar). (b) Arrhenius plots for simulated and experimental N_2O decomposition, obtained in a TPR experiment.

dict the finding of the present work, which shows that a partial pressure of water vapor of 406×10^{-9} bar in the feed is required to achieve agreement between the simulated TPR spectrum and the experimentally observed spectrum reported by Wood et al. [31] (see Fig. 4a) over the temperature range of 550 to 773 K. This difference in partial pressures of water vapor in the feed is directly associated with the temperature range over which agreement between theory and experiment is sought and the choice of objective function chosen to fit the simulation to the experimental observation. In the work of Heyden et al. [30], the objective function was $F(P_{H_2O}, f) = \Sigma(1 - P_{N_2}^{sim}/P_{N_2}^{exp})^2$, instead of $F(P_{H_2O}, f) = \Sigma(P_{N_2}^{exp} - P_{N_2}^{sim})^2$, which is used here. The use of the former objective function favors the low-

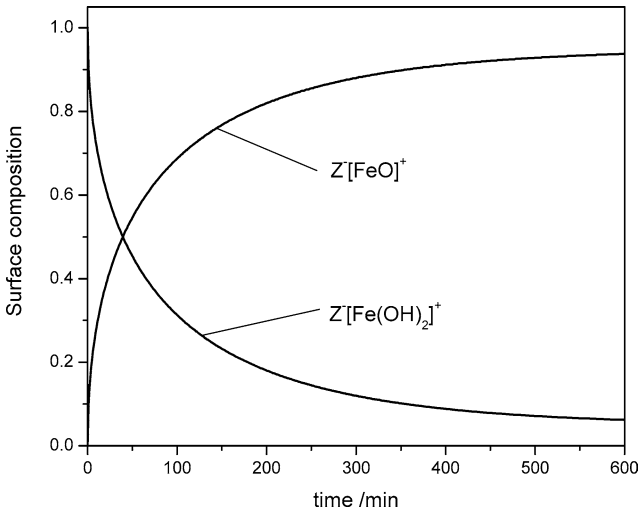

Fig. 5. Simulation of variation of main single iron sites with time during temperature pretreatment of a wet Fe-ZSM-5 catalyst in He. The pretreatment temperature is 773 K and the water pressure in the incoming gas stream is $P_{H_2O} = 406 \times 10^{-9}$ bar.

temperature data, for which the assumption of a steady-state distribution of adsorbed species may not be valid.

Another significant issue is the rate at which a fully hydrated sample of Fe-ZSM-5 undergoes dehydration. A sense of the time required to dehydrate the catalyst can be obtained with the rate parameters listed in Table 1. For this simulation, we assume that the Fe-ZSM-5 is identical to that used in the studies of Wood et al. [31] and, as discussed above, that $f = 0.544$ and the partial pressure of water vapor in the incoming gas stream is 406×10^{-9} bar. Fig. 5 shows that at 773 K it takes about 10 h for an initially hydrated catalyst to achieve a steady-state surface composition. This observation could explain why high-temperature catalyst pretreatment for an extended period of time is found to be important for achieving a high activity for N_2O decomposition [11]. Yet another important point arising from this analysis is that when measurements of N_2O decomposition over Fe-ZSM-5 are carried out by temperature-programmed reaction, the Fe sites will not reach a steady-state distribution with respect to the partial pressure of water vapor in the feed. It is recommended, therefore, that measurements of the rate of N_2O decomposition be made at fixed temperatures that have been maintained for a time sufficient for the catalyst to achieve a steady state with respect to the partial pressure of water in the feed.

3.3. Simulation of transient-response experiments

Wood et al. [31] performed transient-response experiments to investigate the initial stages of the N_2O decomposition. After catalyst pretreatment at 773 K in 3.0% N_2O, the sample was purged in He and then cooled to the temperature of the experiment. During the experiment, 15,000 ppm N_2O in He (60 cm^3/min) was passed through the reactor for 10 min. Then pure He was passed through the reactor for

10 min, after which the feed was switched back to a flow of 15,000 ppm N_2O in He. Transient-response experiments were performed at temperatures of 509, 520, 530, 540, and 588 K.

Since the catalyst surface in these experiments is initially not at steady state with respect to the gas phase, the experiments were simulated with the full reaction mechanism illustrated in Fig. 1 and the rate parameters listed in Table 1. To fit the N_2 partial pressure observed by Wood et al. [31] during the first exposure of the catalyst to N_2O, the initial distribution of single iron sites among $Z^-[FeO]^+$, $Z^-[FeO_2]^+$, and $Z^-[Fe(OH)_2]^+$ was optimized with a sequential quadratic programming (SQP) method [36]. To improve the fit between experimental and simulated N_2 partial pressures, small adjustments were made in the rate parameters. In particular, the activation barrier for N_2O decomposition on $Z^-[FeO]^+$ sites (reactions 4 and 11 in Table 1) was reduced by 6 kcal/mol (without a change in the equilibrium constant) and the activation barrier for N_2O decomposition on $Z^-[OFeO]^+$ sites (reactions 13) was reduced by less than 1 kcal/mol. These small adjustments in the rate parameters had to be made because transient-response experiments are very sensitive to small variations in the rate parameters and the presence of species that show a low activity. Although the first of these adjustments might suggest that the mechanism presented in Fig. 1 is wrong, we do not believe this to be the case. We recall that all activation energies were obtained at the B3LYP/TZVP level of theory with the use of a constrained 5T cluster to represent the Fe site and an associated portion of the zeolite framework, and that the preexponential factors were determined from transition-state theory in the harmonic approximation [30]. Whereas the B3LYP functional is known to underestimate barrier heights by 4–5 kcal/mol [37], use of the harmonic approximation can lead to an overestimation of the preexponential factor by an order of magnitude. As a result the adjustment in the activation barriers for reactions 4 and 11 lies within the limits of accuracy of the rate parameters and the experimental data.

Fig. 6a illustrates both the experimental and the simulated N_2 formation during the first exposure of the catalyst to N_2O at temperatures of 509, 520, 530, and 540 K. In agreement with the experimental observation, no O_2 formation was observed during the whole experiment, and no N_2 formation occurred during re-exposure of the catalyst to N_2O. The initial burst of N_2 production is simulated at all temperatures, with about 18% of the single iron sites or 0.098 (0.18×0.544) of all of the Fe in the zeolite residing initially in the form of $Z^-[FeO]^+$. This latter figure is very close to that reported by Wood et al. [31], 0.10. Fig. 6b shows the evolution of the principal species involving single Fe sites during the experiment carried out at 540 K. The fraction of Fe sites in the form of $Z^-[Fe(OH)_2]^+$ stays constant during the exposure to N_2O, whereas the fraction of Fe sites present as $Z^-[FeO]^+$ decreases and the fraction of Fe sites present as $Z^-[FeO_2]^+$ increases.

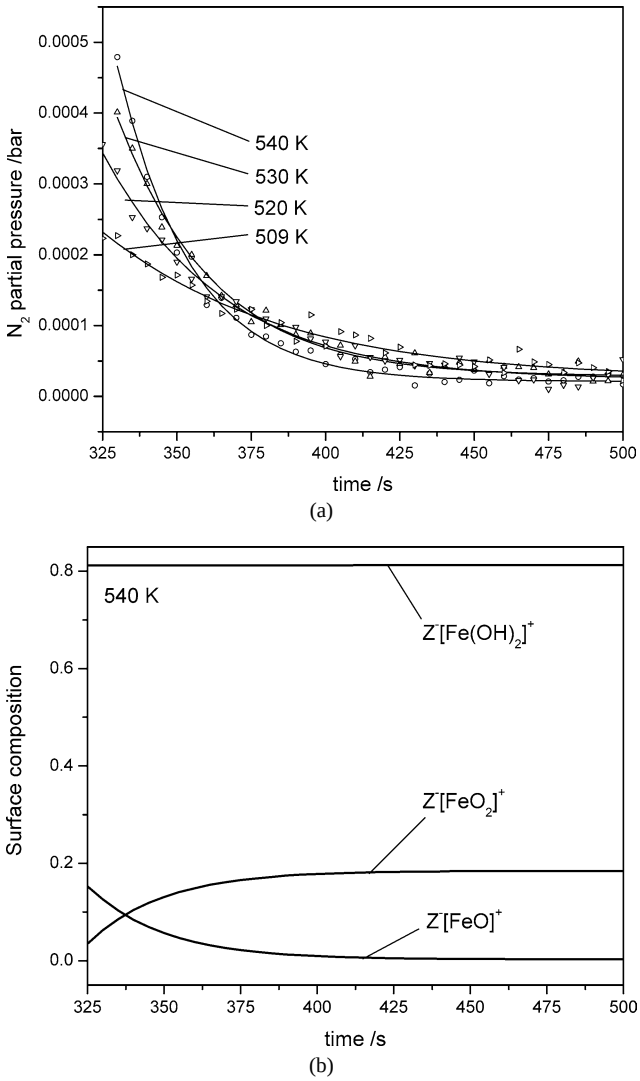

Fig. 6. (a) N_2 formation during transient-response decomposition of 15,000 ppm N_2O in He over Fe-ZSM-5 at various temperatures. The weight of catalyst used was 100 mg and the gas flow rate was 60 cm^3/min. Open symbols are experimental data [31]. Solid lines are simulated data with an optimized initial surface composition. The activation barrier for the N_2O decomposition on $Z^-[FeO]^+$ sites is reduced by 6 kcal/mol. The activation barrier for N_2O decomposition on $Z^-[OFeO]^+$ sites is varied by less than 1 kcal/mol. (b) Distribution of the principal iron-containing species during transient-response decomposition of N_2O upon exposure of the Fe-ZSM-5 to 15,000 ppm N_2O in He at 540 K.

Fig. 7a illustrates the experimental and simulated N_2 and O_2 formation occurring during the transient-response experiment performed for a temperature of 588 K. For this simulation the activation barrier for the N_2O decomposition on $Z^-[FeO]^+$ was reduced by 5.5 kcal/mol, and the barrier for water desorption was reduced by 5.3 kcal/mol. In agreement with experimental observation, a burst of N_2 is observed in the simulations whenever the catalyst is exposed to N_2O. After that, stoichiometric amounts of N_2 and O_2 are formed. The rates of N_2 and O_2 formation do not increase as rapidly with time as the experimentally observed rates, and the activity of the re-exposed catalyst is higher

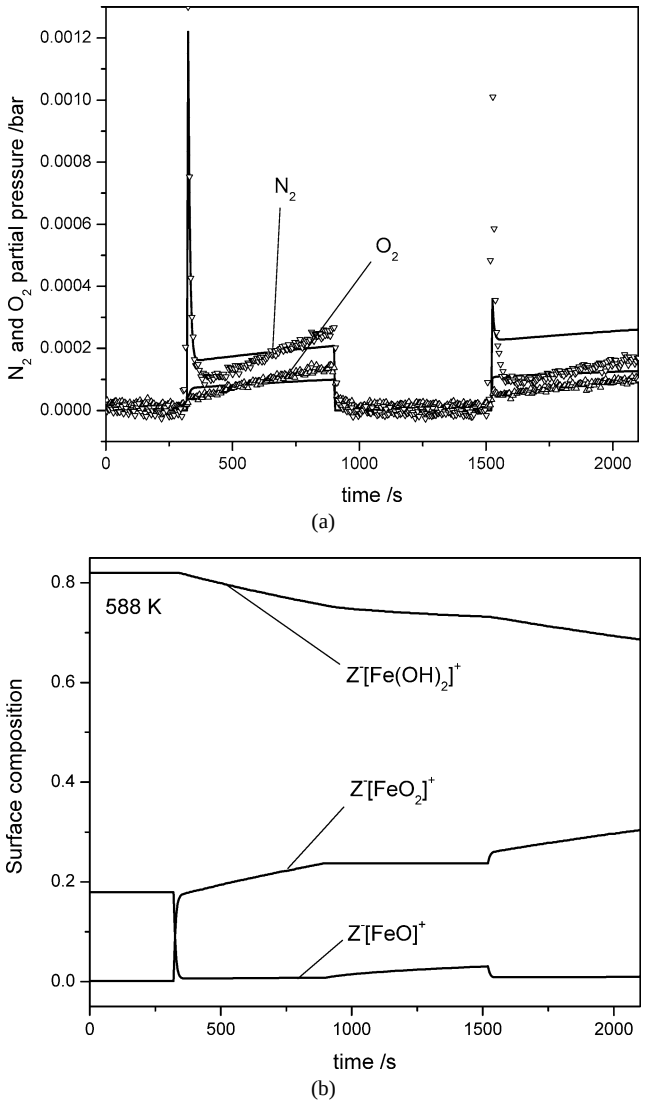

Fig. 7. (a) N_2 and O_2 formation during transient-response decomposition of 15,000 ppm N_2O in He over Fe-ZSM-5 at a temperatures of 588 K. The weight of catalyst used was 100 mg and the gas flow rate was 60 cm^3/min. Open symbols are experimental data [31]. Solid lines are simulated data with an optimized initial surface composition. The activation barrier for the N_2O decomposition on $Z^-[FeO]^+$ sites is reduced by 5.5 kcal/mol; the water desorption barrier is reduced by 5.3 kcal/mol. (b) Distribution of the principal iron-containing species during transient-response decomposition of N_2O upon exposure of the Fe-ZSM-5 to 15,000 ppm N_2O in He at 588 K.

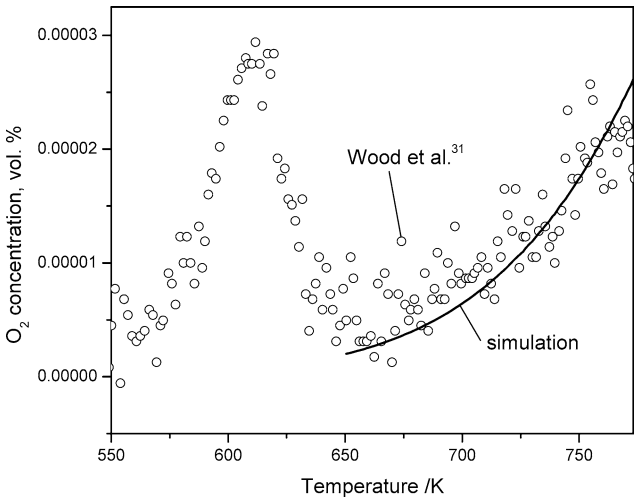

Fig. 8. TPD of O_2 in He from 528 to 773 K following decomposition of 15,000 ppm N_2O in He over Fe-ZSM-5 at 528 K. The weight of catalyst used was 100 mg and the gas flow rate was 60 cm^3/min. The dots correspond to the experimental data, the solid line starting at the beginning of the second TPD peak corresponds to a simulation of O_2 desorption, $Z^-[FeO_2]^+ \rightleftarrows Z^-[Fe]^+ + O_2$, with a by 7 kcal/mol reduced desorption barrier.

for the simulations than that seen experimentally. Nevertheless, the characteristic shape of the curve is in good agreement with the experiments, considering all of the approximations inherent in the simulations. Fig. 7b illustrates the evolution of the principal species involving single Fe sites during the experiment carried out at 588 K. The fraction of Fe sites present as $Z^-[FeO]^+$ decreases sharply during N_2O exposure of the catalyst, causing the fraction of Fe sites present as $Z^-[FeO_2]^+$ to increase. Water slowly desorbs from $Z^-[Fe(OH)_2]^+$, resulting in a further increase in the fraction of Fe sites present as $Z^-[FeO_2]^+$ if N_2O is present and an increase in $Z^-[FeO]^+$ if N_2O is not present in the gas phase. At no time during the experiment is the surface composition at steady state.

In this context it is also important to note that the activation barrier for the elementary step of the first N_2O decomposition on $Z^-[FeO]^+$ ($E^\ddagger = 30.4$ kcal/mol) is 10 kcal/mol higher than the activation barrier of the second N_2O decomposition on $Z^-[FeO_2]^+$ ($E^\ddagger = 20.1$ kcal/mol). On the other hand, the product of the equilibrium constant for N_2O adsorption and the rate constant for N_2O dissociation, $K_{ads}k_{reac}$, is 100 times larger for the first N_2O decomposition on $Z^-[FeO]^+$ (reactions 3 and 4) than for the second N_2O decomposition on $Z^-[FeO_2]^+$ (reactions 5 and 6) for temperatures below 600 K [30].

3.4. Oxygen adsorption and desorption from Fe-ZSM-5

The role of oxygen desorption during N_2O decomposition on Fe-ZSM-5 has been the subject of controversy in the literature. The absence of an inverse dependence on O_2 partial pressure for the rate of N_2O decomposition has led a number of authors to conclude that O_2 desorption is rapid and irreversible and consequently not rate limiting [1,2,9,38]. The results of Heyden et al. [30] and those of the present study also support this conclusion. The absence of a dependence on O_2 partial pressure in the rate expression for N_2O decomposition seen in Eq. (1) is a consequence of the small heat of adsorption for O_2 (0.6 kcal/mol) and the small activation barrier for O_2 desorption (8 kcal/mol). Isotope exchange experiments reported by Nobukawa et al. [39] also support the conclusion that O_2 desorption is facile. Nevertheless, several authors [6,11,31–33,40] have suggested that O_2 desorption is an energetically demanding step and

could be rate limiting. This conclusion was based on NO-assisted N_2O decomposition experiments by Mul et al. [32] and Pérez-Ramírez et al. [33] and on the observation of a high-temperature O_2 desorption peak during temperature-programmed desorption carried out after a sample of Fe-ZSM-5 had been used for N_2O decomposition in the absence of added NO [6,11,31]. Fig. 8 shows an example of such an experiment taken from the work of Wood et al. [31]. Since the activation barrier estimated for the irreversible O_2 desorption was calculated to be 45.7 kcal/mol, which is close to the apparent activation barrier for N_2O decomposition, 44.2 kcal/mol, the authors concluded that the desorption of O_2 could be rate limiting. The theoretical analysis of N_2O decomposition presented by Heyden et al. [30] suggests that the O_2 peak observed by Wood et al. [31] is not likely to arise from the process leading to O_2 formation during steady-state decomposition of N_2O, but, more likely, is due to O_2 release from a species such as $Z^-[FeO_2]^+$ or some other Fe-containing species.

The amount of O_2 desorbed in the first peak seen in Fig. 8 corresponds to about 1.3% of the Fe sites estimated to be present as isolated Fe in the sample of Fe-ZSM-5 used by Wood et al. [31] (0.013 O_2/Fe_{total}). This amount is significantly smaller than the total amount of oxygen deposited in the transient-response experiments, estimated to be about 0.1 O/Fe_{total}, leading us to suspect that the first O_2 desorption peak seen in Fig. 8 results from some minority Fe species. To further support this conclusion, we note that simulation of O_2 desorption from $Z^-[FeO_2]^+$ using the rate parameters given in Table 1 and Ref. [30] (species in the quartet and sextet state were considered) places the peak position at $\sim$ 900 K rather than 675 K. Since a number of authors have observed a second O_2 TPD peak at a temperature of 900 K [6,11,39,41], an effort was made to simulate the second desorption peak seen in Fig. 8. As discussed earlier, the concentration of water vapor in the feed and the fraction of single iron sites in the catalyst were derived from a fit of the simulation of the TPR experiment shown in Fig. 4a. Fig. 8 shows very good agreement between simulation and experiment for an optimized distribution of isolated Fe sites of 20.1% $Z^-[FeO]^+$, 49.5% $Z^-[FeO_2]^+$, and 30.4% $Z^-[Fe(OH)_2]^+$, and an activation barrier for O_2 desorption (reaction 8) that is reduced by 7 kcal/mol relative to the value given in Table 1 (54.2 kcal/mol). Since Wood et al. [31] terminated their TPD experiment at 773 K, it was not possible to assess whether the simulation of O_2 desorption from $Z^-[FeO_2]^+$ would describe the full peak. A TPD experiment similar to that of Wood et al. [31] has been reported by Kiwi-Minsker et al. [11], but in this instance the experiment was carried out to 1100 K. As seen in Fig. 9, the simulation of O_2 desorption from $Z^-[FeO_2]^+$ is in very good agreement with the experimentally observed peak temperature and width reported by Kiwi-Minsker et al. [11]. What is also remarkable is that the peak intensity and area of the simulated and observed peaks agree as well.

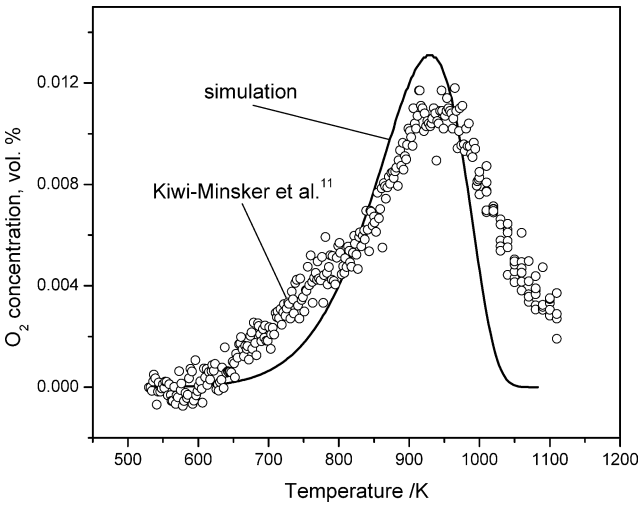

Fig. 9. TPD of oxygen after its deposition from N_2O (523 K) on an iron ZSM-5 catalyst and after irreversible adsorption of water vapor at 523 K. The simulation is the continuation of the TPD simulation illustrated in Fig. 8. No fit parameter was used to match the experimental data of Kiwi-Minsker et al. [11].

The findings of Pirngruber and Roy [42] can also be reconciled with the results of the present study. These authors found a statistical isotope distribution of the O_2 produced during N_2O decomposition by using a feed of 5000 ppm N_2O in He and repeated pulses of 1% $^{18}O_2$ into the N_2O flow; from this they argued that N_2O decomposition could not occur via a Rideal–Eley mechanism. The mechanism presented in Fig. 1 suggests that isotopic scrambling of O_2 could readily be explained by the interaction of O_2 with $Z^-[FeO]^+$. Rapid exchange of O atoms in $Z^-[FeO]^+(O_2)$, formed by this interaction, would lead to a statistical isotope distribution without the need to invoke the concept of a slow O_2 desorption process. In this context it is worth noting that if O_2 desorption were rate limiting, the catalyst surface would be saturated with oxygen atoms and a N_2O decomposition would be zero order in N_2O partial pressure, in contrast to all experimental findings, which show that the rate of N_2O decomposition is first order in N_2O.

4. Conclusions

Several transient-response experiments for the decomposition of N_2O over Fe-ZSM-5 have been simulated from first principles and compared with experimental results. It is shown that the reaction mechanism shown in Fig. 1, together with the rate coefficients listed in Table 1, provides a satisfactory basis for simulating all of the experimental work reported in the literature. The overall rate of N_2O decomposition is found to be first order in N_2O partial pressure and zero order in O_2 partial pressure. The presence of H_2O in the feed gas inhibits the rate of N_2O decomposition by deactivating the active sites required for this process. Site deactivation occurs via the process $Z^-[FeO]^+ + H_2O \rightleftarrows Z^-[Fe(OH)_2]^+$,

which is reversible, and, consequently, the influence of water vapor is strongly temperature dependent. Because of the high activation barrier for H_2O desorption, dehydration of a hydrated sample of Fe-ZSM-5 can take as long as 10 h at 773 K. The presence of low concentrations of water vapor in the feed stream (ppb to ppm levels) affects the measured values for the apparent activation energy and preexponential factor, and this explains the large spread in values reported in the literature, as well as the appearance of an apparent compensation effect. Finally, it is shown that the desorption of O_2 observed at ~ 900 K in TPD experiments conducted after the use of Fe-ZSM-5 for N_2O decomposition is due to the process $Z^-[FeO_2]^+ \rightleftarrows Z^-[Fe]^+ + O_2$; however, this process is not kinetically relevant during steady-state decomposition.

Acknowledgments

The authors appreciate helpful discussions with Dr. Benjamin R. Wood, Dr. Gerhard D. Pirngruber, and Dr. Lioubov Kiwi-Minsker. This work was supported by the Methane Conversion Cooperative funded by BP, the "Fonds der chemischen Industrie," and the Max-Buchner-Forschungsstiftung.

Supplementary material

The online version of this article contains additional supplementary material.

Please visit DOI: 10.1016/j.cat.2005.04.003.

References

[1] G.I. Panov, V.I. Sobolev, A.S. Kharitonov, J. Mol. Catal. 61 (1990) 85.
[2] F. Kapteijn, G. Marbán, J. Rodriguez-Mirasol, J.A. Moulijn, J. Catal. 167 (1997) 256.
[3] G.I. Panov, A.K. Uriarte, M.A. Rodkin, V.I. Sobolev, Catal. Today 41 (1998) 365.
[4] C. Sang, C.R.F. Lund, Catal. Lett. 70 (2000) 165.
[5] E.M. El-Malki, R.A. van Santen, W.M.H. Sachtler, Microporous Mater. 35–36 (2000) 235.
[6] E.M. El-Malki, R.A. van Santen, W.M.H. Sachtler, J. Catal. 196 (2000) 212.
[7] C. Sang, C.R.F. Lund, Catal. Lett. 73 (2001) 73.
[8] B.R. Wood, J.A. Reimer, A.T. Bell, J. Catal. 209 (2002) 151.
[9] Q. Zhu, B.L. Mojet, R.A.J. Janssen, E.J.M. Hensen, J. van Grondelle, P.C.M.M. Magusin, R.A. van Santen, Catal. Lett. 81 (2002) 205.
[10] J. Pérez-Ramírez, F. Kapteijn, J.C. Groen, A. Doménech, G. Mul, J.A. Moulijn, J. Catal. 214 (2003) 33.
[11] L. Kiwi-Minsker, D.A. Bulushev, A. Renken, J. Catal. 219 (2003) 273.
[12] J. Pérez-Ramírez, F. Kapteijn, G. Mul, J.A. Moulijn, Appl. Catal. B 35 (2002) 227.
[13] J. Pérez-Ramírez, F. Kapteijn, G. Mul, J.A. Moulijn, Chem. Commun. 8 (2001) 693.
[14] R. Joyner, M. Stockenhuber, J. Phys. Chem. B 103 (1999) 5963.
[15] A.A. Battiston, J.H. Bitter, D.C. Koningsberger, Catal. Lett. 66 (2000) 75.
[16] A.A. Battiston, J.H. Bitter, F.M.F. de Groot, A.R. Overweg, O. Stephan, J.A. van Bokhoven, P.J. Kooyman, C. van der Spek, G. Vankó, D.C. Koningsberger, J. Catal. 213 (2003) 251.
[17] A.A. Battiston, J.H. Bitter, W.M. Heijboer, F.M.F. de Groot, D.C. Koningsberger, J. Catal. 215 (2003) 279.
[18] A.A. Battiston, J.H. Bitter, D.C. Koningsberger, J. Catal. 218 (2003) 163.
[19] P. Marturano, L. Drozdová, A. Kogelbauer, R. Prins, J. Catal. 192 (2000) 236.
[20] P. Marturano, L. Drozdová, G.D. Pirngruber, A. Kogelbauer, R. Prins, Phys. Chem. Chem. Phys. 3 (2001) 5585.
[21] J. Jia, Q. Sun, B. Wen, L.X. Chen, W.M.H. Sachtler, Catal. Lett. 82 (2002) 7.
[22] S.H. Choi, B.R. Wood, J.A. Ryder, A.T. Bell, J. Phys. Chem. B 107 (2003) 11843.
[23] S.H. Choi, B.R. Wood, A.T. Bell, M.T. Janicke, K.C. Ott, J. Phys. Chem. B 108 (2004) 8970.
[24] K.A. Dubkov, N.S. Ovanesyan, A.A. Shteinman, E.V. Starokon, G.I. Panov, J. Catal. 207 (2002) 341.
[25] J. Pérez-Ramírez, G. Mul, F. Kapteijn, J.A. Moulijn, A.R. Overweg, A. Doménech, A. Ribera, I.W.C.E. Arends, J. Catal. 207 (2002) 113.
[26] E.J.M. Hensen, Q. Zhu, M.M.R.M. Hendrix, A.R. Overweg, P.J. Kooyman, M.V. Sychev, R.A. van Santen, J. Catal. 221 (2004) 560.
[27] Q. Zhu, R.M. van Teeffelen, R.A. van Santen, E.J.M. Hensen, J. Catal. 221 (2004) 575.
[28] J. Pérez-Ramírez, M.S. Kumar, A. Brückner, J. Catal. 223 (2004) 13.
[29] G.D. Pirngruber, M. Luechinger, P.K. Roy, A. Cecchetto, P. Smirniotis, J. Catal. 223 (2004) 13.
[30] A. Heyden, B. Peters, A.T. Bell, F.J. Keil, J. Phys. Chem. B 109 (2005) 1857.
[31] B.R. Wood, J.A. Reimer, A.T. Bell, M.T. Janicke, K.C. Ott, J. Catal. 224 (2004) 148.
[32] G. Mul, J. Pérez-Ramírez, F. Kapteijn, J.A. Moulijn, Catal. Lett. 77 (2001) 7.
[33] J. Pérez-Ramírez, F. Kapteijn, G. Mul, J.A. Moulijn, J. Catal. 208 (2002) 211.
[34] G.D. Pirngruber, M. Luechinger, P.K. Roy, A. Cecchetto, P. Smirniotis, J. Catal. 224 (2004) 429.
[35] P.K. Roy, G.D. Pirngruber, J. Catal. 227 (2004) 164.
[36] Numerical Algorithms Group Fortran Library, Mark 19, NAG GmbH, Garching, Routine: E04FYF (fit), E04UNF (SQP).
[37] Y. Zhao, N. González-García, D.G. Truhlar, J. Phys. Chem. A 109 (2005) 2012.
[38] Y.-F. Chang, J.F. McCarty, Catal. Lett. 34 (1995) 163.
[39] T. Nobukawa, S. Tanaka, S. Ito, K. Tomishige, S. Kameoka, K. Kunimori, Catal. Lett. 83 (2002) 5.
[40] G.D. Pirngruber, J. Catal. 219 (2003) 456.
[41] B.R. Wood, private communication.
[42] G.D. Pirngruber, P.K. Roy, Catal. Lett. 93 (2004) 75.